Physics Faculty Research & Creative Works   Physics

Differential Cross Sections For State-selective Electron Capture In 25100-keV Proton-helium Collisions

D. R. Schultz

C. O. Reinhold

Ronald E. Olson
Missouri University of Science and Technology, olson@mst.edu

D. G. Seely

Differential cross sections for state-selective electron capture in 25–100-keV proton-helium collisions

D. R. Schultz,* C. O. Reinhold,† R. E. Olson, and D. G. Seely‡

Laboratory for Atomic and Molecular Research, University of Missouri–Rolla, Rolla, Missouri 65401
and Department of Physics, University of Missouri–Rolla, Rolla, Missouri 65401

Cross sections differential in the scattering angle of the projectile are presented for electron capture summed over all states and to the 2s, 2p, 3s, 3p, 4s, and 4p states of hydrogen in 25-, 50-, and 100-keV proton-helium collisions. The classical-trajectory Monte Carlo (CTMC) technique was employed for these calculations as well as to compute total cross sections as a function of impact energy. The latter are compared with experiment to display the behavior of the integral state-selective cross sections in this energy regime. Detailed comparison is also made between the calculated angular differential cross sections and the experimental measurements of Martin et al. [Phys. Rev. A **23**, 285 (1981)] for capture summed over all states and of Seely et al. [Phys. Rev. A **45**, R1287 (1992)] for capture to the 2p state. Very good overall agreement is found. Regarding the cross section for capture summed over all states, an improved agreement is demonstrated by using an alternate representation of the initial state in the CTMC method, which improves the electronic radial distribution but which cannot presently be applied to state-selective determinations.

PACS number(s): 34.70.+e

I. INTRODUCTION

In the study of ion-atom collisions, recent trends toward more stringent tests of theory and experimental technique have led from considering the reaction cross section summed over all final states and integrated over all scattering angles (i.e., total cross sections) to cross sections in which some or all of these degrees of freedom are distinguished. In so doing a greater amount of detail is revealed about the collision and a deeper level of understanding may be attained. Concerning specifically the fundamentally important instance of charge transfer in proton-helium collisions, experiment has evolved from simply measuring the rate of production of hydrogen to determining the distributions of the scattering angles of this product, the quantum levels (n, l, m_l) to which the capture proceeds and of both selectively. Motivated by these studies, the purpose of the current work is to present calculations of the angular differential cross section for state-selective (n, l) charge transfer in intermediate energy (25–100-keV) proton-helium collisions. These differential cross sections are shown to provide a more sensitive probe of the theoretical model of charge transfer than total cross sections alone and are particularly relevant due to the recent advent of measurements with which to compare them.

However, it should also be noted that even though such measurements are becoming available, the agreement among theories and experiments is not yet satisfactory regarding all of the less detailed cross sections. As a case in point, Hippler et al. [1] have stated that some of their recent measurements have been stimulated by a rather large disagreement, which existed as to the total cross section for capture to both the ground and 2p states of hydrogen in low-energy proton-helium collisions. This discrepancy persisted even though excellent agreement

between theory and their experiment [1, 2] was obtained over a wide range of impact energies for both the integral and differential alignment of $H(2p)$, a quantity sensitive to the relative m_l populations. As might be expected, the history of the measurement and calculation of some quantities is quite rich. For example, the total cross section for capture in proton-helium collisions was experimentally determined at least as early as 1954 by Stedeford and Hasted [3], whose measurements were extended and repeated in the late 1950s and 1960s [4] as well as quite recently [5–8]. The first quantum-mechanical calculations of capture were made in 1928 and 1930 by Oppenheimer [9] and Brinkman and Kramers [10] using the Born approximation. Since then, more elaborated distorted-wave and coupled-channel models have been developed. A review of the experimental or theoretical developments in the study of charge transfer, even limited to intermediate energy proton-helium collisions is beyond the scope of the present work. Here we concentrate on exploring the ability of classical dynamics to describe the electron capture process as well as on the insight that is gained using this type of approach. In order to place into context the differential cross sections presented in Sec. V, we begin by illustrating the degree of agreement with experiment of the state-selective total cross sections (Sec. IV) calculated using the same theoretical treatment, after a brief description of the theoretical and experimental methods used here (Secs. II and III).

II. THEORETICAL METHOD

The classical-trajectory Monte Carlo (CTMC) technique is a simulation of an ion-atom collision in which a large ensemble of initial electronic configurations is sampled in order to mimic the quantum-mechanical position and momentum distributions, and therefore the

wave function, of an atom. The subsequent motion of the projectile ion, target core and the electron(s) is determined by iterative solution of the classical Hamilton equations. After the integration has been carried out into the asymptotic regime, knowledge of the positions and momenta of the particles allows the scattering angles and energies of the free particles, and the binding energies and orbital angular momenta of the bound particles, to be determined. This method, originally considered by Abrines and Percival [11] and subsequently developed by a number of authors, is described fully elsewhere [12, 13]. Consequently, the details of its implementation are not repeated here except those that are particularly salient to the present work.

In order to explore the sensitivity of our results to the choice of the representation of the initial state, we have utilized a number of models. The initial electronic phase space distribution, $f(r, p; t = 0)$, is constructed in the CTMC approximation so that certain properties of the unperturbed atomic wave function may be reproduced. In particular, it would be desirable to reproduce as well as possible the quantum-mechanical position and momentum distributions simultaneously. That is, we would like to require that

$$\int f(\mathbf{r}, \mathbf{p}; t = 0)d\mathbf{p} \equiv \rho(\mathbf{r}) \sim | \phi(\mathbf{r}) |^2 \tag{1}$$

and

$$\int f(\mathbf{r}, \mathbf{p}; t = 0)d\mathbf{r} \equiv \tilde{\rho}(\mathbf{p}) \sim | \tilde{\phi}(\mathbf{p}) |^2, \tag{2}$$

where $\rho(\mathbf{r})$ and $\tilde{\rho}(\mathbf{p})$ are the position and orbital linear momentum distributions and $\phi(\mathbf{r})$ and $\tilde{\phi}(\mathbf{p})$ are the coordinate and momentum representation of the initial unperturbed wave function.

To simulate the hydrogen atom, Abrines and Percival [11] used the so-called microcanonical distribution in which all initial electronic configurations in the ensemble satisfy the relation

$$f(r, p; t = 0) = \kappa \delta(H - E), \tag{3}$$

where κ is a constant chosen so that the distribution is normalized to unity, E is the binding energy, and H is the electronic Hamiltonian,

$$H = \frac{p^2}{2\mu} + V(r), \tag{4}$$

with μ the reduced mass of the electron and V its interaction with the target nucleus. This function has the property that the resulting distribution of orbital linear momenta coincides exactly with the quantum-mechanical distribution for ground-state atomic hydrogen (see Percival and Richards [12] and references therein). However, the resulting distribution of orbital radii differs substantially from the quantum result, since in the classical model of the atom there exists a maximum radius, given by the balance of kinetic and potential energy, beyond which the electronic orbit cannot extend. Thus, the radial probability density displays a cutoff at this radius.

For atoms or ions with more than one electron, the screening due to the presence of the other electrons must be taken into account. This is usually accomplished by making use of an effective Coulomb potential,

$$V_{\text{eff}} = Z_{\text{eff}}/r, \tag{5}$$

where the effective charge, $Z_{\text{eff}} = Z - s$, is given by subtracting a constant screening s from the nuclear charge Z. Alternately, a model potential V_{mod}, which takes into account the variation of this screening with electronic position, may be utilized. In these cases, neither the momentum nor position distributions may coincide exactly with what would be obtained from a quantum wave function.

Despite these shortcomings, the microcanonical distribution is still by far the most widely used initial distribution in CTMC calculations. As is well known among practitioners, but not too widely documented, a reasonably good representation of the momentum distribution, which is provided even in these cases by the microcanonical distribution, is sufficient to provide a good model for ionization. Percival and Richards [12] have even stated that they considered the radial distribution not to be as important. As we demonstrate later and as has been noted by other authors, it turns out that the position distribution is critical to the details of charge transfer. Other works have also indicated that for certain regimes of ejected electron energy, the radial distribution might also be very important to the mechanism of ionization.

Models that have sought to improve upon this situation by finding methods to sample some function that do a better job representing simultanously the radial and momentum distribtuions have been made by Eichenauer, Grün, and Scheid [14], Hardie and Olson [15], Cohen [16], Blanco et al. [17], and Schmidt, Horbatsch, and Dreizler [18], for example. In the present case in which we wish to find an initial phase-space distribution to model the helium atom, we follow the method of Blanco et al. [17], which is based largely on the ideas of Cohen [16]. This method, which relies on utilizing a spread of binding energies, is also closely related to the technique of Hardie and Olson [15], which utilized a superposition of microcanonical distributions with various energies and weights to fit the radial and momentum distributions. Difficulties in applying the method of Eichenauer, et al. [14], who used a cut-off Wigner distribution, which is essentially a transformation of the density matrix and also possesses a spread of energies about the expectation value, were discussed by these authors as well as by Cohen. We also note that the method of Schmidt et al. is closely related in that a Wigner-like ansatz which contains a spread of energies is used.

To these ends we seek a distribution that is stationary and is therefore dependent only on constants of motion, specifically the binding energy, $f(E)$. This function may be obtained by solving the integral equation (1). After some convenient substitutions we find that

$$f(E) = \frac{2}{\pi} \int_0^{-E} dx \frac{d^2 g(x)}{dx^2} \sqrt{-E - x}, \tag{6}$$

where $x = -V(r)$ and

$$g(x) = \frac{1}{2\pi\sqrt{2}} \frac{d}{dx} \rho(r(x)).$$ (7)

The potential used here to represent the r-dependent screened interaction of the active electron in helium with the nucleus is given by the parametrized Hartree-Fock model potential of Garvey, Jackman, and Green [19]. Equation (6) may be solved numerically and the result may be sampled [16] to yield the desired initial conditions in the Monte Carlo simulation. We note that this initial distribution in which the radial probability density is improved is known as the CTMC-r distribution, by convention.

The resulting radial, momentum, and energy probability densities are depicted in Fig. 1 along with the corresponding quantities found from the microcanonical distribution, with the electronic motion subject to either an effective Coulomb or model potential, and from the multiple-ζ Hartree-Fock wave function for helium of Clementi and Roetti [20]. Clearly, as indicated by the figure, this distribution yields exactly the quantum-mechanical radial probability density. However, a slight shift to lower momenta is also produced but which is seen to be intermediate between the model potential and effective charge results with the microcanonical distribution. The figure also contrasts the form of the binding-energy probability density with that for the microcanonical case which is a δ function. Thus the cost of improving the radial distribution is the necessity of accepting a distribution of initial binding energies.

Thus, in the present study of proton-helium collisions, we are left with the following choices: (i) use of either screened Coulomb or model potential interactions, (ii) use of microcanonical or CTMC-r initial phase space distributions, and (iii) use of either an independent-electron model or explicit inclusion of both atomic electrons. Since two-electron processes do not strongly affect single charge transfer for proton impact, we adopt the use of the independent-particle model [21, 22]. As is well known, this choice leads to an overestimation of the transfer-ionization cross section, and therefore the sum of single capture and transfer ionization, which is frequently measured experimentally. (This cross section is denoted σ_{10}, the subscripts indicating the entrance and exit charges of the projectile.) However, since transfer-ionization for proton impact in the energy range of 25–100 keV is generally an order of magnitude smaller than single capture, this approximation is not too severe. In addition, the advantage of considering the motion of only one electron is computationally quite great. Since the choice of the effective charge may be considered to a certain degree arbitrary, the use the model potential derived from a quantum treatment of the atom seems preferable. Previous work [23] has shown that for proton impact, the effective-charge model fits the experimental measurements for charge transfer better, but for higher-charge-state projectiles, the model potential results are in better agreement, indicating that the effective charge results for proton impact may be somewhat fortuitous. In addition,
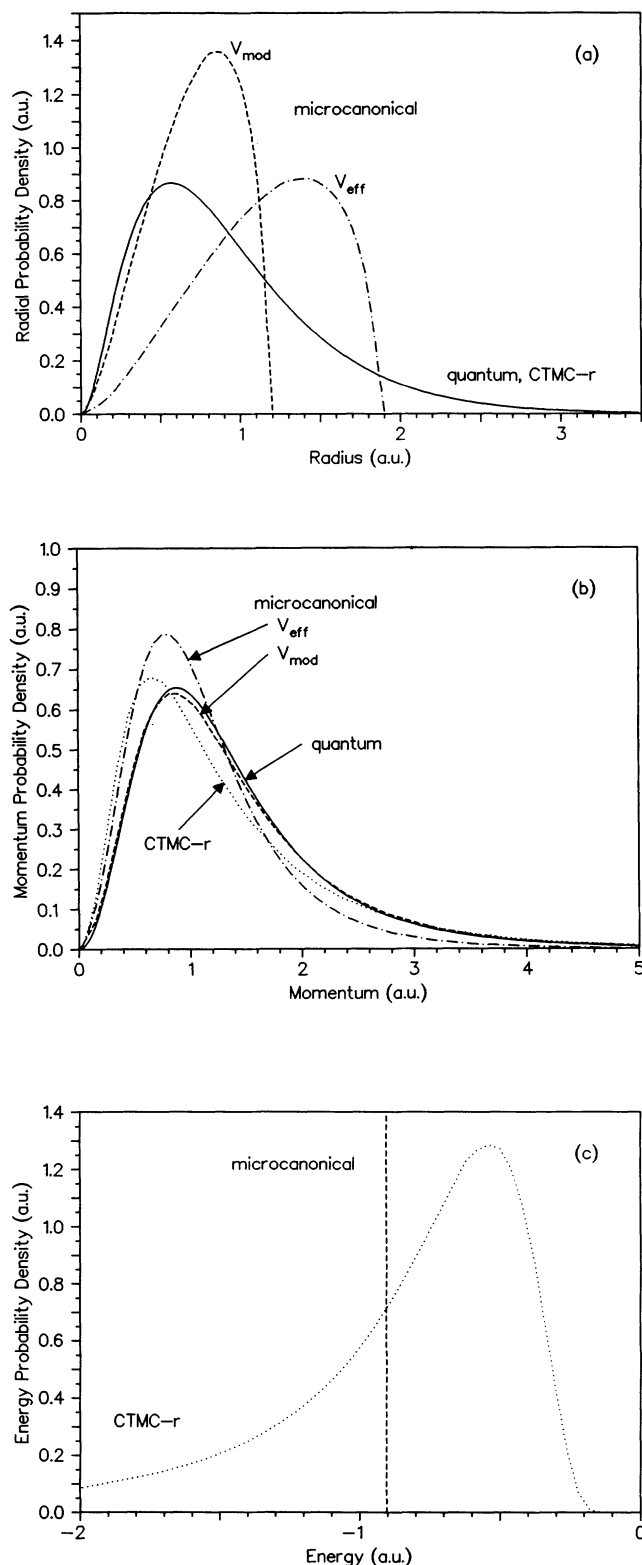

FIG. 1. Electronic radial, momentum, and energy probability densities resulting from the various CTMC models of helium. Comparison is made between microcanonical distributions under both model potential (dashed lines) and Coulomb potential (dot-dashed lines) interactions, the CTMC-r distribution (dotted lines) and the quantum-mechanical (multiple-ζ, Hartree-Fock [20]) result.

since here we wish to consider the angular scattering of the projectile, the model potential allows a more realistic treatment of the projectile-target core interaction. We note that explicit expressions for computing the charge-transfer differential cross sections in the independent-electron model and the CTMC approximation may be found elsewhere [24].

The final choice, that of the initial distribution function, is based on the shortcoming of our ability to analyze the final state after capture in the particle counting method used in the CTMC model. The method of Becker and MacKellar [25], based on a principle of proportionality of classical and quantal weights, is used to identify the product n, l levels after capture from the classical values n_c and l_c given by

$$n_c = \frac{q}{\sqrt{2U}} \tag{8}$$

and

$$l_c = [(x\dot{y} - y\dot{x})^2 + (x\dot{z} - z\dot{x})^2 + (y\dot{z} - z\dot{y})^2]^{1/2}, \tag{9}$$

where q is the charge of the projectile ion, U the product state binding energy, and x, y, and z the Cartesian coordinates of the electron relative to the projectile nucleus after capture. They have shown that

$$[(n-1)(n-\tfrac{1}{2})n]^{1/3} \le n_c \le [n(n+\tfrac{1}{2})(n+1)]^{1/3} \tag{10}$$

determines the correspondence between classical and quantal n levels and

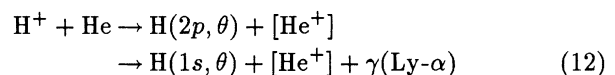$$l \le \left(\frac{n}{n_c}\right) l_c \le l+1 \tag{11}$$

relates the corresponding l levels. These rules have been shown by a number of works to provide a good description of the n, l capture spectrum [23, 25–29] when a microcanonical initial distribution is used. However, our experience in the present work indicates that these rules do not hold when the CTMC-r initial distribution is used. This should be expected since the treatment of the initial and final states is not compatible. That is, the CTMC-r initial state contains a substantial spread of energies and consequently analysis of the product after capture should be treated analogously. In fact, if applied to the initial state, the binning rule for n would even exclude that portion of the initial ensemble corresponding to orbits bound by less than about 0.68 atomic units of energy. To handle the determination of the final n, l level after capture when the CTMC-r distribution is used, a more appropriate method would be to find the overlap of the final n_c, l_c distribution with a series of CTMC-r distributions for each state of the product hydrogen atom. This method would be in complete analogy with what would be done quantum mechanically where projection of the final state onto a basis of hydrogenic wave functions could be performed.

Even if the appropriate CTMC-r distributions were to be found, computing such an overlap would require an extremely large number of events so that the sampling of the final distribution would be of sufficient detail. In con-

trast, the CTMC method is efficient numerically because only a particle counting scheme is necessary to extract cross sections, a task much easier to accomplish than producing a smooth, finely spaced mesh approximation to a function. Consequently, in the face of such difficulties and without an alternate method, we will only consider the CTMC-r initial distribution for cross sections in which we sum over the detailed spectrum of states. Thus, for the total or angular differential cross section for capture summed over all states, we may apply this method, but for state-selective capture, we will be limited to employing the microcanonical initial distribution.

III. EXPERIMENTAL DATA

Experimentally, the angular-differential cross sections for the collision process

$$\begin{aligned} \mathrm{H}^+ + \mathrm{He} &\rightarrow \mathrm{H}(2p, \theta) + [\mathrm{He}^+] \\ &\rightarrow \mathrm{H}(1s, \theta) + [\mathrm{He}^+] + \gamma(\mathrm{Ly}\text{-}\alpha) \end{aligned} \tag{12}$$

were measured with incident proton energies of 25, 50, and 100 keV [30]. The brackets indicate that the final state of the helium ion was not detected. Hydrogen atoms, which were scattered through an angle θ, were detected in coincidence with photons emitted perpendicular to the scattering plane, which had wavelengths in the interval 1140–1400 Å. This radiation is strongly dominated by Ly-α photons emitted in the $2p$ to $1s$ decay, but it was impossible to exclude radiation from the $\mathrm{He}^+(n = 4 \rightarrow n = 2)$ transition, which arises from the possible excitation of the target ion with simultaneous capture, but which is estimated to be only a small contribution [30].

The results were obtained using the 200-kV variable-angle ion accelerator from the University of Missouri–Rolla ion-energy-loss spectrometer [30]. Protons were accelerated, collimated, and focused onto helium in a gas cell. Hydrogen atoms resulting from electron capture were separated from scattered ions by a magnet located after the collision region. The photon detector viewed the collision region perpendicular to the scattering plane. By detecting the hydrogen atoms in coincidence with the emitted Ly-α photons the $\mathrm{H}(2p)$ state formed by electron capture can be selected. For a photon detector positioned perpendicular to the scattering plane the coincidence count rate is proportional to the total $\mathrm{H}(2p)$ differential cross section [31, 32]. In this way relative differential cross sections were obtained. The relative cross sections were normalized to a fit of known total cross sections for $\mathrm{H}(2p)$ capture [33]. Further details of the experimental method may be found in a previous publication [30].

IV. TOTAL CROSS SECTIONS

To illustrate the behavior of the total cross sections for state-selective capture in the energy range of interest for proton-helium collisions, we display in Fig. 2 a comparison of experimental measurements with CTMC calculations using the microcanonical distribution and model
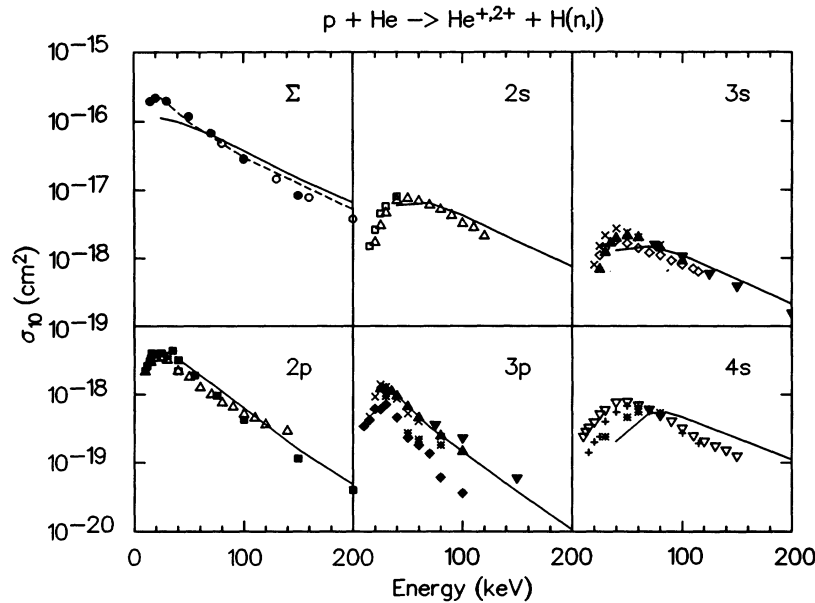
p + He --> He$^{+,2+}$ + H(n,l)

FIG. 2. Total cross section as a function of impact energy for capture into specific states of hydrogen in collisions of protons with helium. The solid curves and dashed curves represent the CTMC results utilizing initial conditions generated subject to either the microcanonical or CTMC-r distributions, respectively, with model potential interactions. The experimental points are as follows: Rudd et al. [5] (solid circles); Shah and Gilbody [6] (open circles); Hughes et al. [35] (open triangles); Andreev, Ankudinov, and Bobashev [36] (open squares); Hippler et al. [2, 1] (solid squares); Lenormand [37] (crosses); Hughes et al. [38] (open diamonds); Ford and Thomas [39] (solid inverted triangles); Brower and Pipkin [40] (stars); Cline, Westerveld, and Risley [41] (solid triangles); Hughes, Dawson, and Doughty [42] (solid diamonds); Doughty, Goad, and Cernosek [43] (open inverted triangles); and Hughes et al. [44] (plus signs).

potential interactions. The theory predicts well the magnitudes and shapes of the measurements in general, and, as shown previously [23], agrees with them at least as well as recent coupled-channel calculations [45]. Similar comparison has been made [23] for proton impact of H_2 with the same good overall agreement with the corresponding experimental measurements of the state-selective total capture cross section.

Also displayed in the figure is our calculation of the total cross section summed over all product states utilizing the CTMC-r initial distribution. Improvement over the result obtained with the microcanonical initial state is evident, especially at the lower impact energies. The origin of this improvement will become apparent when we consider the differential cross section. For higher impact energies, any of the CTMC models, regardless of the initial distribution, will overestimate the total cross section for charge transfer due to the limitations of the classical model of the atom [24,18]. In this case, even at 200 keV the overestimation of the cross section summed over all states is apparent, even though it is not too large in magnitude yet. When the projectile charge is larger, or the product n-level higher, the overestimation will not in general be apparent until higher energies.

V. DIFFERENTIAL CROSS SECTIONS

Differential cross sections clearly reveal more information about the collision process under study than do total cross sections alone. However, in the CTMC method there is a severe computational price which must be paid.

As in an experiment, since the cross section is determined by the number of counts detected in a particular small angular range, a large overall number of events needs to be considered because the total number will be distributed over some larger range. Furthermore, if not only the scattering angle is to be determined but also what specific reaction has occurred, in this case charge transfer to particular n, l levels, the number of detected particles is further reduced. It may be shown that a calculation of the differential cross section for low-lying excited states after capture at intermediate energies requires on the order of 100 times as much computer time as the calculation of the cross section summed over all states and integrated over angles. Previously, since experimental measurements of the angular differential cross section were available only summed over all states (i.e., the measurements of Martin et al. [34, 46]), detailed CTMC calculations were performed just for this case. Reasonable agreement between these previous experiments and calculations was obtained (for proton-atomic hydrogen collisions [47, 27] and for proton-helium collisions [48] using an effective charge model). Therefore, with the demonstrated favorable comparison with total cross sections for capture to specific n, l-levels and for the differential cross section summed over all states, the next logical test of the theory is the study of state-selective differential cross sections. Also, with the recent measurements of capture to the $2p$ state in proton-helium collisions, a significant comparison is possible.

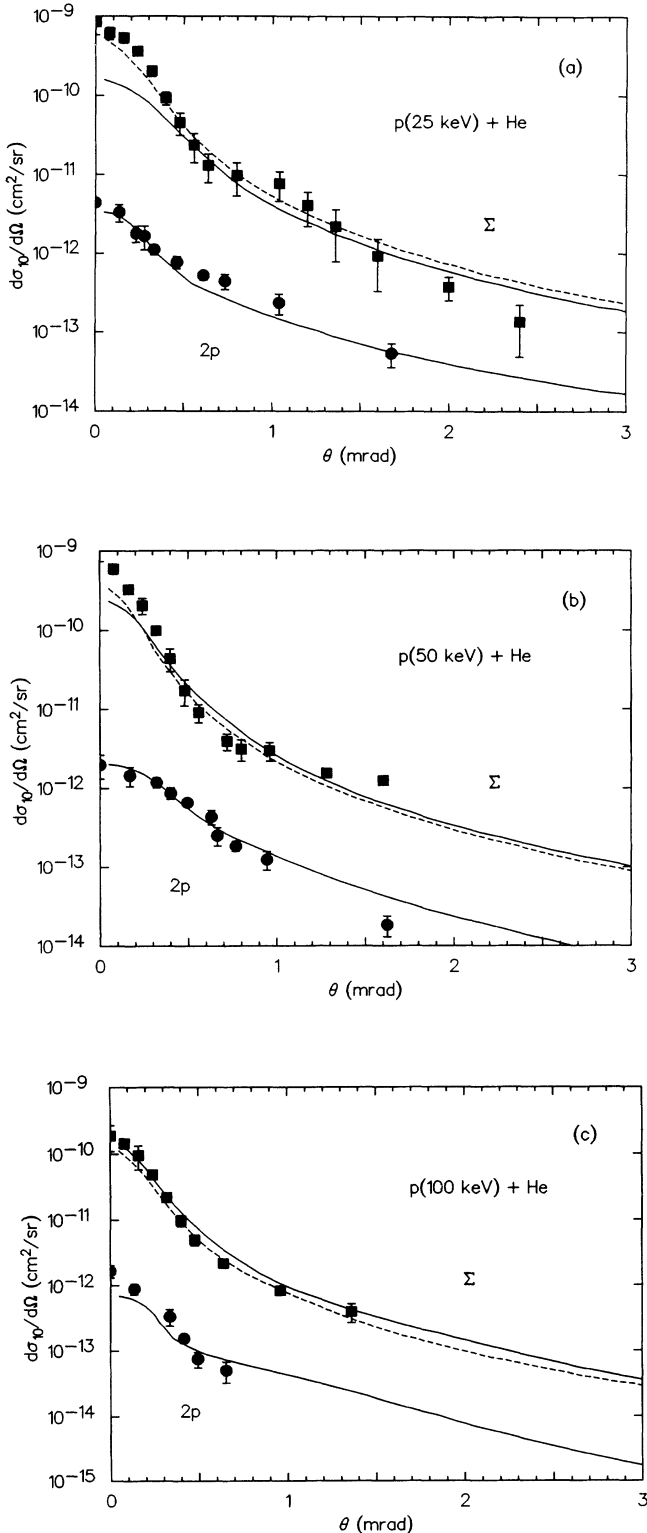In Fig. 3 we display the result of our three-body,

FIG. 3. Differential cross section as a function of laboratory scattering angle for capture to $H(2p)$ and summed over all states for 25-, 50-, and 100-keV proton-helium collisions. The experimental measurements are those of Martin *et al.* [34] (squares) and Seely *et al.* [30] (circles), and the theoretical curves are given by the model potential, microcanonical CTMC (solid lines) and CTMC-r (dashed lines) approximations.

model potential, microcanonical CTMC calculations for the charge-transfer cross section differential in the scattering angle of the projectile for 25-, 50-, and 100-keV proton-helium collisions. The curves indicate the cross section for capture (single capture plus transfer ionization) summed over all states and for the $2p$ state. Also included in the figure are the experimental measurements of Martin *et al.* [34] for capture summed over final states and the very recent measurements of Seely *et al.* [30] in which capture to the $2p$ state has been determined by a coincidence technique, briefly described above.

Comparison of these results with the summed cross section are generally good, especially at 100 keV where the agreement is excellent. At the lower energies, the most significant discrepancies occur for small scattering angles, the difference being largest for the smallest angles and for the lowest impact energy. Especially considering the difficulty of the coincidence experiment performed, the agreement between the calculated and measured $2p$ differential cross sections is extremely good, better in fact than the agreement for the summed cross section in that the deviations do not seem to be systematic.

Since the total cross section, and therefore the number of available capture events, diminishes as the proton energy is raised from 25 to 100 keV, on the order of 5×10^5, 10^6, and 2×10^6 Monte Carlo trajectories were required to obtain the differential cross sections depicted at these three energies. The statistical errors in the calculation of the summed cross sections are typically 1%, or less at the smallest angles, and rise to about 5% at the largest angles (3 mrad). For capture to the $2p$ state, these statistical errors range from about 5% at small angles to 25% at the largest angles. The angular bin size used was 0.1 mrad and the curves were smoothed slightly for plotting.

Considering the good agreement in magnitude and shape between the CTMC and experimental $2p$ results, the divergence of the calculated summed cross section from the measurements at small angles and low impact energies is at first somewhat surprising. Marked improvement over this situation is found, however, when the CTMC-r initial distribution is used. The result of this calculation is also included in Fig. 3. As described above, lacking a suitable method to determine the final captured state in this case, we have limited consideration to the summed cross section. Inspection of these curves indicates that not only is the total cross section improved in this energy range (see Fig. 2) but the problem at small angles is also ameliorated in large part. This comparison indicates that the difference must have its origin in the fact that the radial distribution is cut off in the microcanonical model. As may be readily established the small-angle scattering events come from large-impact-parameter collisions; therefore, if the electron density is cut off, this portion of the spectrum will be cut off rather sharply. The impact-parameter dependence of the capture process shows this to be the case. Thus, by providing a good description of the radial distribution, especially concerning the large radial tail, the CTMC-r model greatly improves the small-angle behavior of the calculated cross section. This effect also evidently accounts for the improved behavior of the total cross section noted above.

In addition, the way in which the capture probability changes with increasing impact energy shows that its range is shorter for higher impact energy. Thus, as the calculations indicate, the greatest effect of this improved distribution at large radial distances is for the low-energy collisions. We also note that the impact-parameter dependence of capture to the 2p, and the higher excited levels, is much shorter ranged than for capture to the ground state, which dominates the summed cross section. Therefore, since there is electron density at these much smaller radial distances, even in the microcanonical model, the excited-state capture is not underestimated at small angles. We see that the CTMC-r and microcanonical models produce complimentary results, dependent upon whether or not the process possesses a strong dependence on the large radius component of the orbital distribution. Clearly, other processes such as excitation and ionization should be affected for certain conditions in a similar way.

Also arising from the impact-parameter-dependence difference between capture to the ground and excited states is the difference between the shapes of the summed (mostly 1s) and 2p differential cross sections. Both the experimental and theoretical results indicate that the 2p cross section is not as strongly peaked at very small angles as the summed cross section. Since the capture to the 2p state comes from much smaller impact parameters than the 1s state, the shape is flatter due to the scattering occurring primarily in the internuclear potential. For the large-impact-parameter component of the 1s capture cross section, deflection of the projectile is less strongly affected by the internuclear interaction due to the screening by the electrons.

Another way to look at this behavior is to consider the differential cross section as being determined by the product of the the impact-parameter-dependent probability of capture multiplied by the elastic differential cross section for the scattering of the proton by the helium atom, i.e.,

$$\frac{d\sigma_{10}}{d\Omega} \propto P_{10}(b)\frac{d\sigma^{elastic}}{d\Omega}, \tag{13}$$

where $b = b(\Omega)$ is the impact parameter and $d\Omega = \sin\theta \, d\theta \, d\phi$ with θ and ϕ the polar and azimuthal scattering angles. From this formula we see that, since the probability for capture to the ground state extends to larger impact parameters than for capture to the 2p state, the ground-state differential cross section will be much more peaked near 0 mrad. We emphasize that this prescription is only approximate since, for example, the impact parameter is not in general given in a one-to-one correspondence with the scattering angle. It has been demonstrated at intermediate energies [49] that the shape and magnitude of the differential cross section for capture summed over all states in proton-hydrogen collisions can be reproduced utilizing a modified CTMC technique by separating the nuclear and electronic motions. In the present study, we have opted to perform the complete three-body simulation since no benchmark was already in existence for excited-state capture differential cross sections in the models under consideration. Moreover, the

use of a central potential has been shown to be invalid for energies as low as 500 keV for proton-helium collisions [50]. A useful adjunct study would be to explore the applicability of the alternate method to excited-state capture.

Finally, in Fig. 4 we display the results of the present calculation for all the excited states in which a sufficient
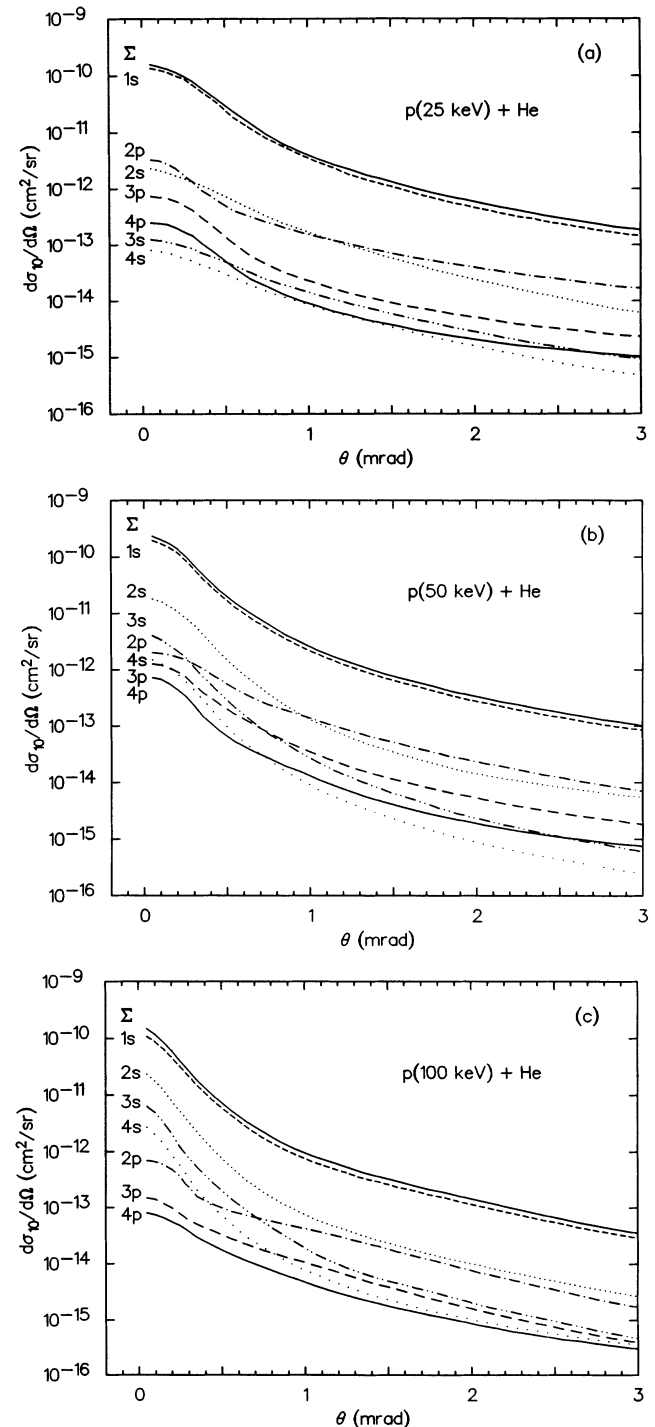

FIG. 4. Cross section for capture to specific n, l states of hydrogen differential in the laboratory scattering angle for 25-, 50-, and 100-keV proton-helium collisions in the model potential, microcanonical CTMC approximation.

number of events were obtained in the simulations to report a statistically meaningful differential cross section. One sees immediately from the figure that, as expected, capture to the ground state is the dominant component and that the other states (including capture to levels in which too few events were present to display a result) sum to an approximately constant factor. Also readily noticed is the fact that the cross sections for the various levels are not ordered in the same way for each impact energy. In general, the cross sections are ordered from greater to lesser in magnitude by increasing n level, but the changing dominance of the l levels complicates this simple scheme. For example, at 25-keV proton energy and at small angles, the ordering is ($1s$, $2p$, $2s$, $3p$, $4p$, $3s$, $4s$) indicating that $l = 1$ is preferred over $l = 0$. However, at 100 keV, the l dependence changes and the order is ($1s$, $2s$, $3s$, $4s$, $2p$, $3p$, $4p$). Thus at high impact energy we observe a dominance of capture to s states over capture to p states.

The trend of this behavior with impact energy arises from the changing overlap in momentum space of the initial and captured traveling states. That is, since capture is dependent on the matching of the electron and projectile velocities the probability is largest when the momentum distribution of the captured level, translated by the projectile velocity, overlaps to the greatest extent with the initial electronic momentum distribution. At very low impact velocity, the projectile-centered p-state momentum distribution has a larger overlap with the initial-state distribution than the s state. As impact velocity is increased, the translation required to boost the electron to the projectile frame shifts the distributions to higher momentum and the s states, with their long tails in momentum space, have a larger overlap than p states. This behavior is manifested in the total cross sections, as may be seen in Fig. 2 where the p-state total cross sections are larger than those for the corresponding s states at the lowest energies displayed, but then drop off more rapidly with increasing impact energy than the s-state cross sections.

Regarding the differential cross sections specifically, not only is there a change in overall magnitude of the cross sections with angular momentum as a function of impact energy, but also a change in the shapes of the angular distributions depending on l. This behavior is due to the change in impact-parameter dependence with collision energy of the capture process leading to states with $l = 0$ and 1. At the highest energies displayed, capture may proceed more readily at larger impact parameters for s states than for p states. This leads to the observed situation that the cross section for capture to s states is more forwardly peaked than for capture to p states

at small angles, as may also be inferred from Eq. (13) and the behavior of the capture probability as a function b and l. This is essentially the same behavior we have noted in comparing the shapes of the $2p$ and $1s$ cross sections in the discussion of Fig. 3.

Furthermore, both the experimental measurement of the angular distribution of capture to the $2p$ state and the theoretical calculations for all the p states indicate that at an angle of about 0.4 mrad a change of slope occurs in the cross section, differing substantially from the shape of the s-state cross sections. The Coulomb-Brinkman-Kramers calculations of Burgdörfer [51] for protons colliding with helium at about 56 keV indicate that this feature of the differential cross section may be due to the way in which the different shapes of the $2p_x$ and $2p_0$ subshell cross sections add.

VI. CONCLUSIONS

In summary, we have calculated state-selective total and differential cross sections for charge transfer in intermediate-energy proton-helium collisions. As previously shown, good overall agreement exists between the results of the classical trajectory Monte Carlo technique and the existing experimental measurements of total n and l resolved cross sections and differential cross sections summed over the product states. Better agreement has been found in the present work regarding the total cross section summed over n and l by using an improved initial representation of the target electronic radial distribution. This model also improves the agreement at very small scattering angles in the differential cross section due to the improved representation at large electronic radii. Application of this model to state-selective cross sections is not presently possible due to the incompatibility of the initial distribution and the existing methods of determining the bound states after capture in the CTMC approximation. Finally, excellent agreement has been shown between the results of the conventional CTMC model and very recent experimental measurements of the differential cross section for capture to the $2p$ state. Results for other low-lying states have been displayed and their shape and magnitude dependence on l described.

ACKNOWLEDGMENTS

---

* Present address: Physics Division, Oak Ridge National Laboratory, Oak Ridge, TN 37831-6373.
† Present address: Department of Physics, University of Tennessee, Knoxville, TN 37996.
‡ Present address: Physics Department, Albion College, Albion, MI 49224.

[1] R. Hippler, W. Harbich, H. Madeheim, H. Kleinpoppen, and H.O. Lutz, Phys. Rev. A 35, 3139 (1987).
[2] R. Hippler, W. Harbich, M. Faust, H.O. Lutz, and L.J. Dubé, J. Phys. B 19, 1507 (1986).

[3] J.B.H. Stedeford and J.B. Hasted, Proc. R. Soc. London Ser. A **227**, 466 (1954).

[4] For a bibliography of these experiments, see Oak Ridge National Laboratory Report No. 5206, 1977.

[5] M.E. Rudd, R.D. DuBois, L.H. Toburen, C.A. Ratcliffe, and T.V. Goffe, Phys. Rev. A **28**, 3244 (1983).

[6] M.B. Shah and H.B. Gilbody, J. Phys. B **18**, 899 (1985).

[7] M.B. Shah, P. McCallion, and H.B. Gilbody, J. Phys. B **22**, 3037 (1989).

[8] W.K. Wu, B.A. Huber, and K. Wiesemann, At. Data Nucl. Data Tables **42**, 157 (1989).

[9] J.R. Oppenheimer, Phys. Rev. **31**, 349 (1928).

[10] H.C. Brinkman and H.A. Kramers, Proc. Acad. Sci. Amsterdam **33**, 973 (1930).

[11] R. Abrines and I.C. Percival, Proc. Phys. Soc. **88**, 861 (1966).

[12] I.C. Percival and D. Richards, Adv. At. Mol. Phys. **11**, 1 (1975).

[13] R.E. Olson and A. Salop, Phys. Rev. A **16**, 531 (1977).

[14] D. Eichenauer, N. Grün, and W. Scheid, J. Phys. B **14**, 3929 (1981).

[15] D.J.W. Hardie and R.E. Olson, J. Phys. B **16**, 1983 (1983).

[16] J.S. Cohen, J. Phys. B **18**, 1759 (1985).

[17] S.A. Blanco, C.A. Falcón, C.O. Reinhold, J.I. Casaubón, and R.D. Piacentini, J. Phys. B **20**, 6295 (1987).

[18] A. Schmidt, M. Horbatsch, and R.M. Dreizler, J. Phys. B **23**, 2327S (1990).

[19] R.H. Garvey, C.H. Jackman, and A.E.S. Green, Phys. Rev. A **12**, 1144 (1975).

[20] E. Clementi and C. Roetti, At. Data Nucl. Data Tables **14**, 177 (1974).

[21] J.M. Hansteen and O.P. Mosebekk, Phys. Rev. Lett. **29**, 1361 (1972).

[22] J.H. McGuire and L. Weaver, Phys. Rev. A **16**, 41 (1977).

[23] L. Meng, C.O. Reinhold, and R.E. Olson, Phys. Rev. A **42**, 5286 (1990).

[24] D.R. Schultz, C.O Reinhold, and R.E. Olson, Phys. Rev. A **40**, 4947 (1989).

[25] R.L. Becker and A.D. MacKellar, J. Phys. B **17**, 3923 (1984).

[26] R.E. Olson, Phys. Rev. A **24**, 1726 (1981).

[27] R.E. Olson, Phys. Rev. A **27**, 1871 (1983).

[28] R.E. Olson and D.R. Schultz, Phys. Scr. **T28**, 71 (1989).

[29] J. Pascale, R.E. Olson, and C.O. Reinhold, Phys. Rev. A **42**, 5305 (1990).

[30] D.G. Seely, S.W. Bross, A.D. Gaus, J.W. Edwards, D.R.

Schultz, T.J. Gay, J.T. Park, and J.L. Peacher, Phys. Rev. A **45**, R1287 (1992).

[31] J. Macek and D.H. Jaecks, Phys. Rev. A **4**, 2288 (1971).

[32] R.H. McKnight and D.H. Jaecks, Phys. Rev. A **4**, 2281 (1971).

[33] Oak Ridge National Laboratory Report No. 6086/V1 (1990).

[34] P.J. Martin, K. Arnett, D.M. Blankenship, T.J. Kvale, J.L. Peacher, E. Redd, V.C. Sutcliffe, and J.T. Park, Phys. Rev. A. **23**, 2858 (1981).

[35] R.H. Hughes, H.R. Dawson, B.M. Doughty, D.B. Kay, and C.A. Stigers, Phys. Rev. **146**, 53 (1966).

[36] E.P. Andreev, V.A. Ankudinov, and S.V. Bobashev, in *Abstracts of Papers of the Fifth International Conference on the Physics of Electronic and Atomic Collisions, Lennigrad, 1967*, edited by I.P. Flaks *et al.* (Nauka, Leningrad, 1967), p. 309.

[37] J. Lenormand, J. Phys. **37**, 699 (1976).

[38] R.H. Hughes, E.D. Stokes, Song-Sik Choe, and T.J. King, Phys. Rev. A **4**, 1453 (1971).

[39] J.C. Ford and E.W. Thomas, Phys. Rev. A **5**, 1694 (1972).

[40] M.C. Brower and F.M. Pipkin, Phys. Rev. A **39**, 3323 (1989).

[41] R.A. Cline, W.B. Westerveld, and J.S. Risley, Phys. Rev. A **43**, 1611 (1991).

[42] R.H. Hughes, H.R. Dawson, and B.M. Doughty, Phys. Rev. **164**, 166 (1967).

[43] B.M. Doughty, M.L. Goad, and R.W. Cernosek, Phys. Rev. A **18**, 29 (1978).

[44] R.H. Hughes, C.A. Stigers, B.M. Doughty, and E.D. Stokes, Phys. Rev. A **1**, 1424 (1970).

[45] A. Jain, C.D. Lin, and W. Fritsch, Phys. Rev. A **36**, 2041 (1987).

[46] P.J. Martin, D.M. Blankenship, T.J. Kvale, E. Redd, J.L. Peacher, and J.T. Park, Phys. Rev. A **23**, 3357 (1981).

[47] D. Eichenauer, N. Grün, and W. Scheid, J. Phys. B **15**, L17 (1982).

[48] D.R. Schultz and R.E. Olson, Phys. Rev. A **38**, 1866 (1988).

[49] N. Toshima, T. Ishihara, A. Ohsaki, and T. Watanabe, Phys. Rev. A **40**, 2192 (1989).

[50] R. Dörner, J. Ullrich, H. Schmidt-Böcking, and R.E. Olson, Phys. Rev. Lett. **63**, 147 (1989).

[51] J. Burgdörfer, Ph.D. thesis, Freien Universität Berlin, 1981.